Journal of Power Sources 194 (2009) 662–667

Contents lists available at ScienceDirect

Journal of Power Sources

journal homepage: www.elsevier.com/locate/jpowsour

Conductive area ratio of multiblock copolymer electrolyte membranes evaluated by e-AFM and its impact on fuel cell performance

Naohiko Takimoto[a,*], Shogo Takamuku[b], Mitsutaka Abe[b], Akihiro Ohira[a], Hae-Seung Lee[c], James E. McGrath[c]

[a] FC-Cubic, National Institute of AIST, Aomi 2-41-6, Koto-ku, Tokyo 1350064, Japan
[b] Fuel Cell Laboratory, Nissan Research Center, Nissan Motor Co., Ltd., Yokosuka, Kanagawa 2378523, Japan
[c] Department of Chemistry, Virginia Polytechnic Institute and State University, Blacksburg, VA 24060, USA

ARTICLE INFO

Article history:
Received 6 March 2009
Received in revised form 27 April 2009
Accepted 16 June 2009
Available online 24 June 2009

Keywords:
Multiblock copolymers
Fuel cell performance
Electrochemical atomic force microscopy
Conductive area ratio
Polymer electrolyte membrane

ABSTRACT

The correlation between membrane surface morphology and fuel cell performance was investigated using a series of hydrophilic–hydrophobic multiblock copolymers based on poly(arylene ether sulfone) with different block lengths. The proton conductive regions on the membrane surface were successfully observed by using electrochemical atomic force microscopy (e-AFM). The results revealed a strong dependence of the hydrophilic/hydrophobic microphase-separated structure on the block length. The conductive area ratio (CAR) estimated from the proton conduction image decreased as the block length increased, and it was found to be closely connected with cell resistance that determines fuel cell performance. The well-defined phase-separated structure of multiblock copolymers can improve proton conductivity without any undesirable increments in water uptake or swelling, but in some instances, it affects the interfacial connection with the catalyst layer, resulting in lower fuel cell performance. The results of this study suggest the necessity for further improvement of the membrane morphology by optimizing both the casting conditions and the molecular design of the block sequences.

1. Introduction

Fuel cells have attracted much attention as promising alternative power generators owing to their advantages of high energy efficiency, noiseless operation, and environmental friendliness as compared with present energy sources. Among the various types of fuel cells, polymer electrolyte fuel cells (PEFCs) are expected to be used in many applications, such as power sources for vehicles, residential co-generation systems, and portable electronic devices [1].

Polymer electrolyte membranes (PEMs), which are one of the most important components of PEFCs, have a wide range of characteristic requirements: high proton conductivity at low humidity, high gas barrier, and high mechanical and chemical stabilities. Among the various types of PEM, hydrocarbon-based (HC-type) polymers have been extensively studied as an alternative to Nafion, which is one of the most widely used PEM materials, from the viewpoints of cost, environmental friendliness, and stability at high temperatures [2,3]. Although HC-type membranes show excellent properties superior to Nafion under a fully hydrated condition, they have significantly lower proton conductivity at lower relative humidity (RH). Building multiblock copolymers using various types of sulfonated and non-sulfonated aromatic hydrocarbon monomers is one approach that has been studied to overcome this drawback. Some improvement has been reported due to the unique hydrophilic/hydrophobic phase-separated structure that enhances the self-diffusion coefficient of water and might enhance proton and water transport [4–7].

The impact of the monomer structures and the block length on the membrane morphology and properties has been extensively reported, but the effect on fuel cell performance has rarely been discussed in the literature. While multiblock copolymers have a well-ordered hydrophilic/hydrophobic phase-separated structure, there are considerable non-conductive hydrophobic regions at the surface simultaneous with the hydrophilic proton conductive networks. Such regions presumably act as barriers to the mass transfer of protons and water at the membrane–catalyst layer interface in membrane electrode assemblies (MEAs). Unfortunately, their unique surface and/or internal morphologies observed by conventional atomic force microscopy (AFM), transmission electron microscopy (TEM), and scanning electron microscopy (SEM) have not been correlated with proton conduction through the membrane. Thus, a new method is needed for directly distinguishing the proton conductive and non-conductive regions of the surface. Recently, we succeeded in simultaneously observing the proton conduction and surface morphology of PEMs using a unique method

* Corresponding author. Tel.: +81 3 3599 8553; fax: +81 3 3599 8554.
E-mail address: nao-takimoto@aist.go.jp (N. Takimoto).

0378-7753/$ – see front matter © 2009 Elsevier B.V. All rights reserved.
doi:10.1016/j.jpowsour.2009.06.045

called e-AFM, an AC-mode AFM coupled with an electrochemical technique, and proved the correlation between the proton conductive areas and the surface morphology [8,9]. Using this observation technique, we can investigate the surface morphology and proton conductive and non-conductive regions related to the phase-separated surface structure of multiblock copolymer membranes.

This present study focused on the impact of the surface morphology of the segmented sulfonated multiblock copolymer membranes on fuel cell performance. A series of multiblock copolymers with different block lengths prepared separately were investigated by using the e-AFM method, and the results revealed a correlation between the hydrophilic/hydrophobic phase-separated surface morphology and the proton conductive/non-conductive regions. It was surprisingly found that the conductive area ratio (CAR) of the membrane decreased with increasing block length. An analysis of fuel cell performance also revealed that cell resistance increased as the CAR decreased, even though there was an increment in proton conductivity.

2. Experimental

2.1. Materials and membrane preparation

A series of multiblock copolymers with disulfonated poly(arylene ether sulfone) hydrophilic blocks (BPSH) and unsulfonated poly(arylene ether sulfone) hydrophobic blocks (BPS), denoted as BPSH*x*–BPS*x* where *x* indicates the block length of both the hydrophilic and hydrophobic sequences, and a random copolymer with BPSH and BPS were synthesized and identified as reported before [6,7,10,11]. Fig. 1 shows the chemical structures of the copolymers discussed in this paper. The copolymers in potassium form were dissolved in NMP (7 wt.%) and filtered through a porous cellulose filter with a 7-μm pore diameter. The solutions were then cast onto clean glass substrates and dried in an oven at 80 °C for 17 h. The membranes were converted to an acid form by immersing them in 1 M hydrochloric acid for 2 days, followed by immersion in deionized water for 2 days. Thickness was measured by micrometer screw gauge at ambient condition, and the membranes of 30 μm (±2 μm) in thickness was used. The IEC values of the membranes were determined by a back titration method monitored by a pH meter.

2.2. Water uptake and proton conductivity measurement

The water uptake of each membrane was determined gravimetrically by using an IGAsorp (Hiden Isochema). The membranes were dried at 80 °C in a dry nitrogen gas flow for at least 5 h, and then equilibrated at the specified RH for at least 30 min before the measurement. The water uptake of the membranes was calculated as

$$\text{Water uptake}\,(\%) = \frac{W_{\text{wet}} - W_{\text{dry}}}{W_{\text{dry}}} \times 100$$

where W_{wet} and W_{dry} are the weights of wet and dry membranes, respectively.

Proton conductivity at 80 °C under partially hydrated conditions was measured in a window cell geometry using a Solartron 1260 Impedance/Gain-Phase Analyzer over the frequency range of 10 Hz to 1 MHz. Membranes were equilibrated in a humidity–temperature oven (TH 203HA, ETAC) at the specified RH and temperature for at least 30 min before the measurement. Proton conductivity of each sample was calculated from dry membrane thickness and membrane resistance taken at the frequency that produced the minimum imaginary response.

2.3. Proton conduction imaging by AFM

AC-mode AFM and proton conduction images were obtained using a JSPM-5400 scanning probe microscope (Nihon Denshi) with a humidity control unit [8,9]. A Pt-coated cantilever (NSC05/Pt_20, NT-MDT) with a force constant of 12 Nm^{-1} and a resonance frequency of 250 kHz was used. A membrane sample was placed on a gold-plated conductive sample stage with Nafion dispersion (DE-2020, DuPont) as adhesives. Before AFM observation, a sample was placed in a humidity controlled chamber for at least 1 h. A bias voltage of −1.6 V was applied to the sample stage during the observation. All the topography, phase, and proton conduction images were simultaneously collected.

Calculation of CAR was carried out using Win-SpmII Processing software (Nihon Denshi). A 10% of the maximum current value detected in a 1 μm scan box was used as threshold. An average value of two different scan areas was obtained for each sample.

2.4. Single fuel cell test

Membrane electrode assemblies (MEAs) were prepared according to the following procedure: each membrane was conditioned under 100% RH for 24 h at room temperature and then assembled with commercial gas diffusion electrodes (ELE0072: HiSPEC9100 catalyst coated on TGP-H-060 carbon paper substrate with perfluorosulfonic acid ionomer, Johnson–Matthey) at 130 °C for 10 min under a pressure of 4 MPa. The active area was 25 cm^2, and Pt catalyst loading was 0.4 mg cm^{-2} for both sides. An MEA was assembled in a single cell between bipolar plates made of graphite with serpentine flow channels and gaskets made of silicone rubber.

A single fuel cell test fed by hydrogen (H_2)/oxygen (O_2) or H_2/air was conducted at a cell temperature of 80 °C under two humidity conditions, 100% for H_2/O_2 and 30% for H_2/air. The stoichiometric ratio (SR) was 1.5/2.0 (anode/cathode). During the test, the current density (A cm^{-2}), cell voltage (V) and high-frequency resistance (HFR, mΩ cm^2) were obtained.

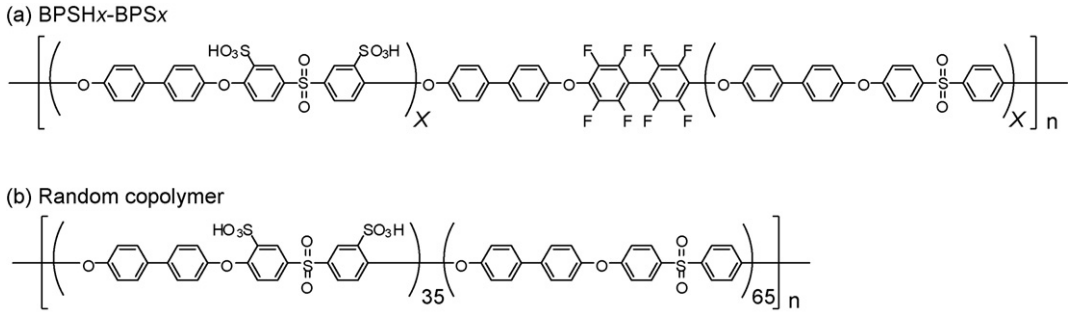

Fig. 1. Chemical structures of (a) BPSH*x*–BPS*x* and (b) random copolymers.

Table 1
Properties of BPSH*x*-BPS*x* and random copolymer.

Sample	Block length (g mol^{-1})	IEC[a] (mequiv. g^{-1})	Water uptake[b] (wt.%)	Proton conductivity[b] (mS cm^{-1})
BPSH3–BPS3	3000	1.45	28	76
BPSH5–BPS5	5000	1.42	27	119
BPSH7–BPS7	7000	1.45	30	130
BPSH10–BPS10	10000	1.49	33	131
Random		1.43	24	40

[a] Measured by back-titration.
[b] In-plane direction, measured at 80 °C, 90% RH.

3. Results and discussion

3.1. Membrane properties

Typical properties such as the ion-exchange capacity (IEC) and proton conductivities of the membranes are summarized in Table 1. As the results in Fig. 2 indicate, the block copolymers clearly showed higher proton conductivity than the random copolymer at all RH conditions. The longer block length apparently achieved higher proton conductivity, in spite of there being no distinct difference in either the IEC or water uptake among all the samples. Therefore, the difference in proton conductivity was ascribed to the microphase-separated structure, as previously reported [7]. In this paper, only the in-plane proton conductivities were presented, but the through-plane direction measurements were also conducted. However, no significant anisotropy of the proton conductivity between those two directions was found.

3.2. Proton conduction imaging by e-AFM

The e-AFM method was used to investigate the microphase-separated surface structure of the multiblock and random copolymer membranes. This method makes it possible to distinguish the active proton conductive regions of the membrane surface by simultaneously collecting the topographic, phase, and proton conduction images with high resolution [8,9]. The images shown in Fig. 3 clearly revealed that the surface patterns reflecting the hydrophilic/hydrophobic microphase separation strongly depended on the block length of the copolymer; the morphological features of the surface became more obvious as the block length increased. In BPSH10-BPS10, having the longest block length, many large projected domains with a worm-like shape were clearly distinguished on the air-side surface, and proton conduction was detected at the exact same position as these domains (Fig. 3e, j, and o). Thus they were assumed to be composed of swollen hydrophilic (rich) domains and connected in the bulk of the membrane, even though they appeared to be isolated from each other on the surface.

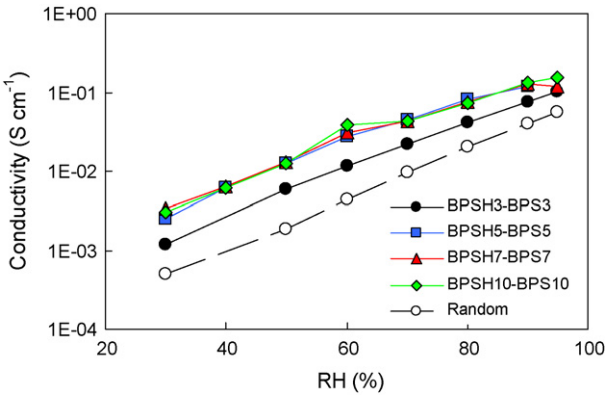

Fig. 2. Proton conductivity of BPSH*x*–BPS*x* and random copolymers at 80 °C.

Non-conductive regions considered to be hydrophobic domains were clearly seen between these hydrophilic domains, and it was observed that hydrophilic/hydrophobic phase separation was distinctly developed.

However, these morphological features seen in the BPSH10–BPS10 membrane gradually disappeared as the block length decreased. In BPSH7–BPS7, the proton conductive region became shorter and narrower compared with that of BPSH10–BPS10, and each conductive region appeared to be less separated (Fig. 3n and s). The surface morphologies of both the BPSH5–BPS5 and BPSH3–BPS3 membranes were more clearly different from that of BPSH10–BPS10; they were composed of small spherical grains instead of worm-like domains, and proton conduction was detected over almost the entire surface, not only at the projected domains but also at the non-projected regions. In addition, the contrast of the conductive regions of the BPSH5–BPS5 and BPSH3–BPS3 was not uniform for each spot (Fig. 3l and m). The contrast in an image indicates the current value detected at each spot and presumably reflects the conductivity of the spot especially near the surface. Therefore, the nonuniform contrast of the image implies the heterogeneity of proton conductivity in each domain. Such phenomena are ascribable to the different level of the microphase separation which depended on the block length. The microphase separation of BPSH3–BPS3 and BPSH5–BPS5 with shorter block lengths was probably less well-developed than that of BPSH7–BPS7 and BPSH10–BPS10. Thus, along with the well-developed hydrophilic domains, many hydrophilic/hydrophobic non-separated (or mixed) domains formed on the surface and worked as weak proton conductive regions. For longer blocks, such incompletely phase-separated domains were not observed at least on the surface because their phase separation was sharply developed. These results agreed with the proton conductivity values (Fig. 2). The sharply developed phase separation seen in BPSH10–BPS10 may have contributed to make proton conduction superior to that for the incompletely developed separation seen in BPSH3–BPS3 and BPSH5–BPS5. Here, it should be noted that the current value observed in this method is not necessarily proportional to the proton conductivity of the bulk membrane, because it depends on the sample conditions such as contact between the membrane and the stage. Therefore, it is very difficult to compare the contrast of the images between different samples, unlike comparing the contrast in one image.

The difference in the surface morphology between the air- and substrate-side was also noteworthy. The substrate-side surface of the BPSH7–BPS7 (Fig. 3n) and BPSH10–BPS10 (Fig. 3t) membranes showed a less developed phase-separated structure compared with the air-side surface. This suggests that the phase separation was determined not only by the block length, but also by the casting conditions such as the drying temperature, substrate materials, concentration and viscosity of the solution, and so on. On the other hand, the morphological features of each observed sample showed no changes against the RH changes between 30% and 90%. The hydrophilic/hydrophobic microphase-separated structure seems to be strongly fixed, and allowed no further rearrangements during hydration/dehydration.

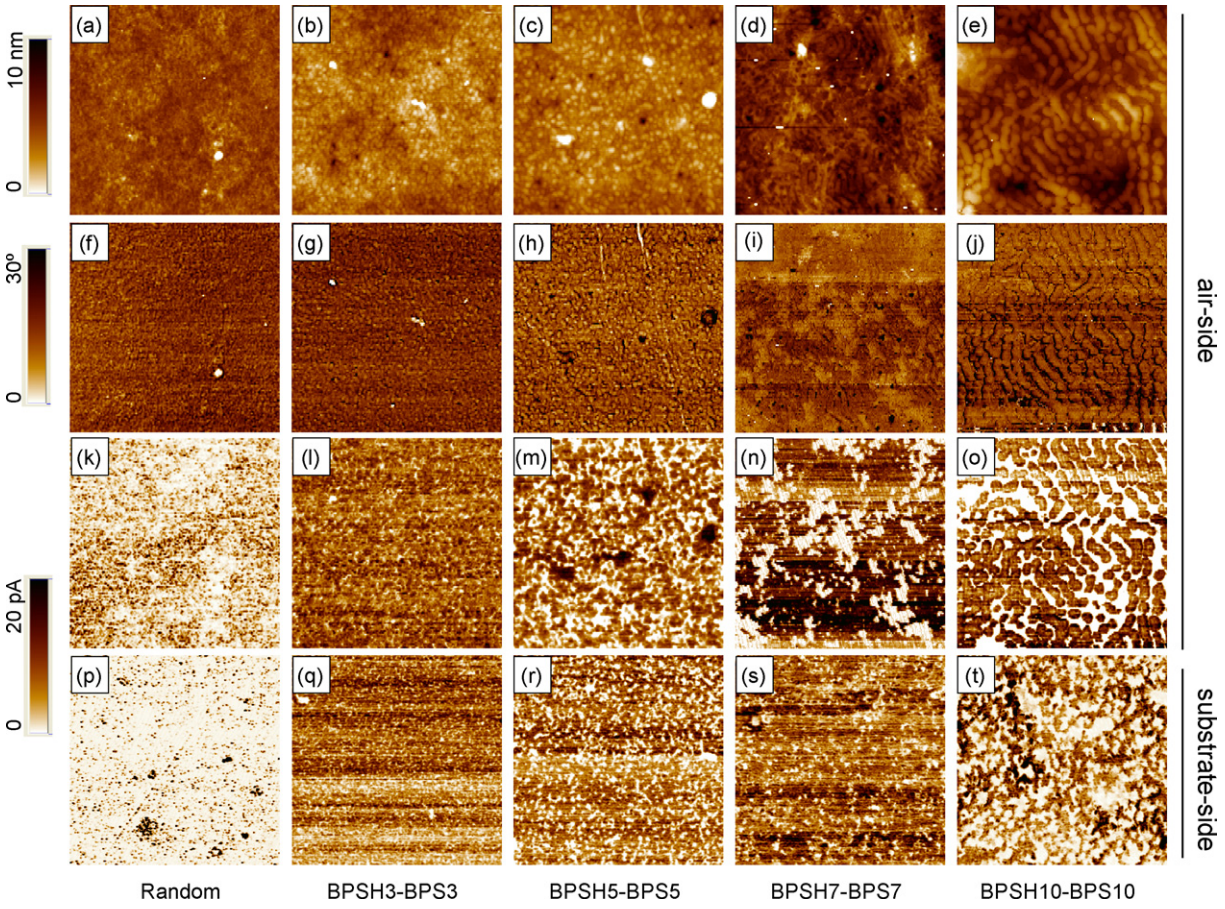

Fig. 3. AFM images of BPSH*x*–BPS*x* and random copolymer membranes at 22 °C, 50% RH. (a–e) Topographic, (f–j) phase, and (k–t) proton conduction images. Scan box 1 μm × 1 μm, bias voltage −1.6 V. Conductive regions are represented as dark.

In order to discuss the difference in surface morphology and activity of each membrane more quantitatively, the CAR was determined from the proton conduction images. The CAR indicates how much of the surface is covered by proton conductive regions that are effectively connected through the bulk of the membrane. As shown in Fig. 4, the CAR roughly tended to decrease as the block length increased. In the BPSH10–BPS10 membrane, the CAR was around 50% for both sides, and it was nearly the same as the molar ratio of the hydrophilic/hydrophobic segments. However, the order of the CAR for BPSH5–BPS5 and BPSH7–BPS7 was not consist with the block length. There might be a threshold point between 5000 and 7000 g mol^{-1} that makes the morphological features different. The surface structure of the BPSH5–BPS5 membrane was similar to that of BPSH3–BPS3, but clearly different from that of BPSH7–BPS7.

Note that the membranes used in this study were prepared under exactly the same casting procedure and conditions, which were not ideally designed for each copolymer. Therefore, there is no assurance that the results described above concerning the membrane properties and surface structure would be obtained for different casting procedures and conditions.

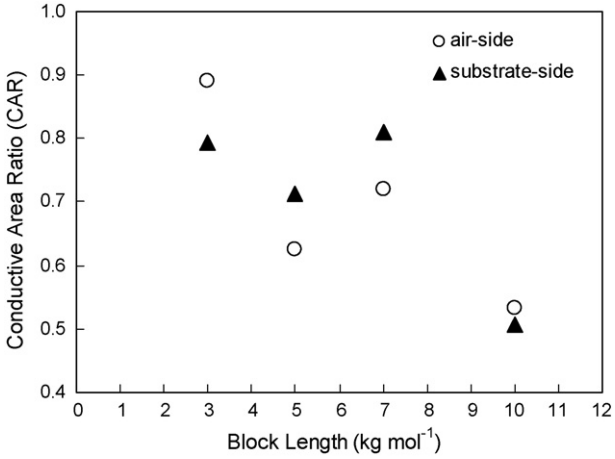

Fig. 4. Comparison of the conductive area ratio (CAR) of BPSH*x*–BPS*x* membranes.

3.3. Fuel cell performance

To investigate the effect of the block length of the multiblock copolymer on fuel cell performance, a series of BPS*x*–BPSH*x* block copolymers and the random copolymer were examined under fully humidified (Fig. 5a) and low RH (Fig. 5b) conditions. For the fully humidified condition, almost the same *I*–*V* curves were obtained for all samples. However, a significant difference in HFR, which signifies the total cell resistance value, was observed between the membranes, and the order of the HFR values was not in agreement with that of the proton conductivities. Surprisingly, the HFR value of BPSH10–BPS10 was the largest in spite of its highest proton conductivity; this membrane was expected to exhibit the lowest HRF value of all. The cell performance under the low RH condition was markedly more different between the membranes; BPSH10–BPS10 with the longest sequence showed poorer performance than any of the other multiblock copolymers. Those differences in fuel cell performance cannot be explained by the difference in proton conductivity, so it is inferred that there were other factors that were

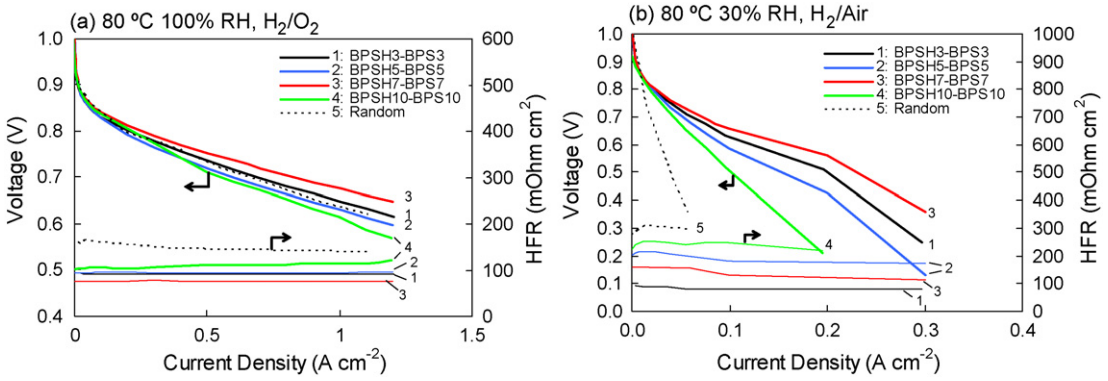

Fig. 5. Fuel cell performance of BPSH*x*–BPS*x* and random copolymers: (a) fully hydrated condition and (b) low RH condition.

Table 2
Contribution of cell resistance.

Sample	CAR[a]	Resistance at 100% RH[b] (mΩ cm^2)			HFR at 30% RH[c] (mΩ cm^2)
		HFR	R_{mem}[d]	$R_{non\text{-}mem}$	
BPSH3–BPS3	0.84	91	39	52	80
BPSH5–BPS5	0.67	95	25	70	183
BPSH7–BPS7	0.76	77	23	54	132
BPSH10–BPS10	0.52	111	23	88	247

[a] Average of air- and substrate-sides.
[b] H_2/O_2, 100% RH.
[c] H_2/air, 30% RH.
[d] Calculate from proton conductivity at 90% RH.

not considered. In order to improve the membranes and/or MEAs, it is essential to understand such factors, which might be the key determinants of fuel cell performance.

The contribution of the resistance components calculated from the proton conductivity of the membrane and the HFR value for each sample is shown in Table 2. To simplify the calculation, cell resistance was divided into two components: the membrane resistance (R_{mem}) calculated from the proton conductivity at 90% RH and the membrane thickness (30 μm), and the non-membrane resistance ($R_{non\text{-}mem}$) which was defined as the difference between HFR and R_{mem}. The contribution of the total cell resistance differed considerably among the samples, and a membrane with a higher HFR value showed a higher $R_{non\text{-}mem}$. For example, BPSH10–BPS10 showed a value of 88 mΩ cm^2, while BPSH3–BPS3 showed a value of 52 mΩ cm^2. Interestingly, the $R_{non\text{-}mem}$ values changed in parallel with the surface morphology of the membrane, although no distinct correlation was seen with either the block length or proton conductivity (Fig. 6). A relation between the CAR determined from the proton conduction images and $R_{non\text{-}mem}$ was clearly seen: $R_{non\text{-}mem}$ increased as the CAR of the membrane surface decreased. Note that the CAR values used here were determined from the proton conduction images obtained at 50% RH, but they were nearly constant against the RH changes from 30% to 90%, as mentioned in the previous section.

According to Pivovar and Kim, the $R_{non\text{-}mem}$ discussed in this paper is thought to include electronic resistance (such as that of the gas diffusion layer, separator, current collector, and so on) and the interfacial resistance between the membrane and the catalyst layer [12]. In this study, electronic resistance was considered to be equal among the samples, so the difference in $R_{non\text{-}mem}$ is only ascribable to the interfacial resistance between the membrane and the catalyst layer. It is quite reasonable for a membrane with a lower CAR to show higher interfacial resistance because of the lack of efficient connections of the proton conductive networks at the boundary between the membrane and the catalyst layer [13]. As the CAR decreased, which means the increments of the

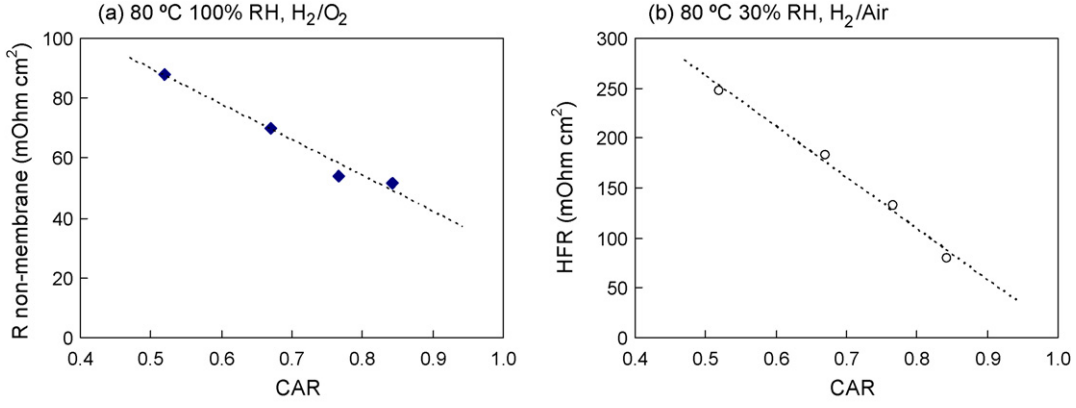

Fig. 6. (a) Non-membrane resistance under fully hydrated condition and (b) HFR at low RH condition versus CAR.

non-conductive regions on the surface, the probability of contact between the conductive regions of the membrane and the ionomer in the catalyst layer decreased. The proton transfer at the interface must be strongly restricted due to the decrements of conductive paths, and it makes the overall resistance between the membrane and the electrode high even if the contact resistance between each contacted region is small.

Such inactive hydrophobic-rich areas presumably affected not only proton conduction but also mass transfer (e.g. that of water) at the membrane–electrode interface. Fuel cell performance under the low RH condition indicated that the HFR value of each membrane was much lower than the R_{mem} expected from the proton conductivities (Fig. 5b). This result may indicate that the membrane inside the MEA was much more hydrated due to the absorption of the water generated during the test; thus the order of the HFR values might reflect the ability of water to move at the interface. Membranes with a higher CAR, such as BPSH3–BPS3 and BPSH7–BPS7, probably absorbed the product water rapidly and efficiently due to the hydrophilic-rich surface, resulting in lower membrane resistance. In contrast, since approximately 50% of the surface of the BPSH10–BPS10 membrane was covered by hydrophobic inactive regions, the movement of the product water may have been strongly restricted. Of course, it is very difficult to predict the fuel cell performance only from the HFR value because it is quite complicated especially at low RH condition. Fig. 5b indicates that the ohmic loss is not the only reason for the difference of the fuel cell performances. However, it must be emphasized that CAR is the predominant factor to the HFR value.

4. Conclusion

The correlation between the hydrophilic/hydrophobic block length and fuel cell performance was investigated using BPSH*x*–BPS*x* multiblock copolymer systems. As the block length increased, proton conductivity increased under all the RH conditions, due to the sharply developed microphase-separated structure that was identified by AFM. In contrast, the order of fuel cell performance was not consistent with the block length. Non-membrane resistance, including interfacial resistance between the membrane and the electrode, was found to increase with a decreasing CAR estimated from the proton conduction images.

For multiblock copolymers, such a phase-separated structure is useful in enhancing proton conductivity without increasing water uptake or swelling, but it sometimes affects the (interfacial) connection with the electrode. That is due to an increase in the non-conductive surface area that might act as barrier to mass transfer. A more detailed study on the mechanism of the surface pattern formation and optimization of the casting conditions is needed to improve the surface morphology. An evaluation of the CAR would be a good indicator of membrane improvement.

Finally, it was found that proton conductivity is a useful property for PEM evaluation, but it does not directly ensure the desired fuel cell performance due to the lack of information about the interfacial connection, especially in the in-plane direction measurement. Through-plane proton conductivity measurement would be a better tool for understanding fuel cell performance more precisely, even though it has still a room for improvement in reproducibility and reliability. We are trying to measure and analyze the through-plane conductivities of the multiblock copolymers with newly designed apparatus and it will be published elsewhere.

Acknowledgements

The Polymer Electrolyte Fuel Cell Cutting-Edge Research Center (FC-Cubic) would like to thank the Ministry of Economy, Trade and Industry of Japan for the financial support. The Virginia Tech group would like to thank the Nissan Motor Co and the US Department of Energy under contract DE-FG-36-06G016038 for support.

References

[1] W. Vielstich, A. Lamm, H. Gasteiger (Eds.), Handbook of Fuel Cells: Fundamentals, Technology, and Applications, Wiley, Hoboken, NJ, 2003.
[2] M.A. Hickner, H. Ghassemi, Y.-S. Kim, B.R. Einsla, J.E. McGrath, Chem. Rev. 104 (2004) 4587–4612.
[3] B. Smitha, S. Sridhar, A.A. Khan, J. Membr. Sci. 259 (2005) 10–26.
[4] Y. Yang, S. Holdcroft, Fuel Cells 5 (2005) 171–186.
[5] J. Meier-Haack, A. Taeger, C. Vogel, K. Schlenstedt, W. Lenk, D. Lehmann, Sep. Purif. Technol. 41 (2005) 207–220.
[6] H.S. Lee, A. Roy, O. Lane, S. Dunn, J.E. McGrath, Polymer 49 (2008) 715–723.
[7] A. Roy, H.S. Lee, J.E. McGrath, Polymer 49 (2008) 5037–5044.
[8] N. Takimoto, A. Ohira, Y. Takeoka, M. Rikukawa, Chem. Lett. 37 (2008) 164–165.
[9] N. Takimoto, L. Wu, A. Ohira, Y. Takeoka, M. Rikukawa, Polymer 50 (2009) 534–540.
[10] F. Wang, M. Hickner, Q. Ji, W. Harrison, J. Mecham, T.A. Zawodzinski, J.E. McGrath, Macromol. Symp. 175 (2001) 387–395.
[11] F. Wang, M. Hickner, Y.-S. Kim, T.A. Zawodzinski, J.E. McGrath, J. Membr. Sci. 197 (2002) 231–242.
[12] B.S. Pivovar, Y.S. Kim, J. Electrochem. Soc. 154 (2007) B739–B744.
[13] T.V. Nguyen, M.V. Nguyen, G. Lin, N. Rao, X. Xie, D.-M. Zhu, Electrochem. Solid-State Lett. 9 (2006) A88–91.